

Beam-foil Spectroscopy of the $1s2s2p^23p\ ^6L$ - $1s2p^33p\ ^6P$ Transitions in O IV, F V and Ne VI

Bin Lin¹, H. Gordon Berry^{1,y}, Tomohiro Shibata¹, A. Eugene Livingston¹, Henri-Pierre Gamier², Thierry Bastin², and J. Desesquelles³

¹ Department of Physics, University of Notre Dame, Notre Dame, IN 46556

² IPNAS, University of Liege, B4000 Liege, Belgium

³ Lab Spectrometrie Ion & Mol, University of Lyon, F-69622 Villeurbanne, France

(Dated: April 17, 2024)

We present observations of VUV transitions between doubly excited sextet states in O IV, F V and Ne VI. Spectra were produced by collisions of an O^+ , $(FH)^+$ and Ne^+ beam with a solid carbon target. Some observed lines are assigned to the $1s2s2p^23p\ ^6L$ - $1s2p^33p\ ^6P$ electric-dipole transitions in O IV, F V and Ne VI, and are compared with results of MCHF (with QED and higher-order corrections) and MCDF calculations. 31 new lines have been identified. The sextet systems of boronlike ions are possible candidates for x-ray and VUV lasers.

PACS numbers: 32.70.-n, 39.30.+w, 31.10.+z, 31.15.Ar

I. INTRODUCTION

The sextet systems of boronlike ions are possible candidates for x-ray and VUV lasers [1], and have been investigated recently. The lowest terms of these systems ($1s2s2p^3\ ^6S$, $1s2s2p^23s\ ^6P$ and $1s2s2p^33d\ ^6P$) have been studied along B I isoelectronic sequence [2, 3, 4]. The studies of higher excited sextet states ($1s2p^33s\ ^6S$) have been lately reported [1]. However, energy level diagrams of these ions are still far from complete. Experimentally, these levels are difficult to observe by conventional spectroscopic techniques, such as high voltage discharge in gas cell method, because these levels lie well above several ionization limits of *ve*-electron singlet states (see Fig. 1). Even though they are metastable against autoionization, they usually de-excite and disappear by collisions with other ions without radiative transitions. Fast beam-foil technique allows straight forward observations of radiative transitions produced by these sextet states [5, 6].

In 1992 beam-foil spectroscopy [2, 3] was used to provide initial data on low-lying sextet states in doubly excited boronlike nitrogen, oxygen and fluorine. Recent work of Lapierre and Knystautas [3] on possible sextet transitions in Ne VI highlights the significance in this sequence. They measured several excitation energies and lifetimes. Fine structures of the $1s2s2p^23s\ ^6P_J$ states were resolved and measured in O IV, F V and Ne VI by Lin and Berry et al [1]. There are no further results reported for transitions from highly excited sextet states.

In some works on beam-foil spectroscopy of sextet states in B I isoelectronic sequence, their identifications show rather weak lines and overwhelming blending prob-

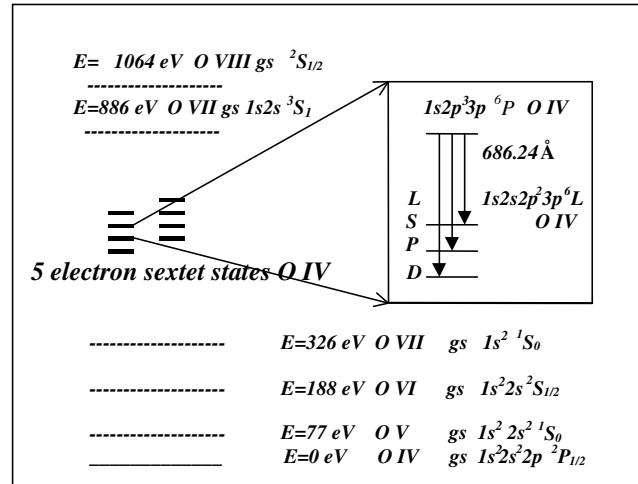


FIG. 1: Term diagram of the doubly excited sextet states of O IV. The mean wavelength for the $1s2s2p^23p\ ^6L$ - $1s2p^33p\ ^6P$ transitions in O IV is shown.

lems. Hence, accurate theoretical studies of sextet states in B I isoelectronic sequence are strongly needed to help identifications. However, theoretical analysis of these *ve*-electron systems is difficult because strong electron correlation, relativistic corrections, and even QED effects have to be included in the calculations [1, 4, 7]. Recent line identifications in the sextet systems were made on the basis of MCHF and MCDF [1, 2, 4, 8] or on the basis of Z-expansion along B I isoelectronic sequence [1, 3]. From these works 6 terms were determined.

The sextet states $1s2s2p^23p\ ^6L$, $L=S, P, D$ and $1s2p^33p\ ^6P$ in B I isoelectronic sequence are well above several ionization levels as shown in Fig. 1, and metastable against electric-dipole radiative decay to singly excited *ve*-electron states and against Coulomb autoionization into the adjacent continuum $1s^22l^2l'n1^4L$ due to different spin multiplicity. Thus, main decay channel is radi-

Electronic address: blin@nd.edu; URL: <http://www.nd.edu/~blin/>

^yElectronic address: Berry.20@nd.edu; URL: <http://www.science.nd.edu/physics/Faculty/berry.html>

tion in fast beam-foil experiments.

In this work, fast beam-foil spectra of oxygen were recorded at Liege using grating incidence spectrometers. Spectra of oxygen and neon were previously recorded at Lyon and Argonne. The $1s2s2p^23p\ ^6L - 1s2p^33p\ ^6P$, $L=S, P, D$ electric-dipole transitions in $O\ IV$, $F\ V$ and $Ne\ VI$ have been searched in these spectra. Comparisons are given with results of MCHF (with QED and higher-order corrections) and MCDHF calculations.

II. EXPERIMENT

The experiments were performed on a standard fast beam-foil excitation system at a Van de Graaff accelerator beam line at the University of Liege [6, 15, 16, 17, 18]. To produce spectra of oxygen in the wavelength region near 660-710 Å a beam current of about 1.3 A of $^{32}O_2^+$ and $^{16}O^+$ ions at a beam energy of 1.5 and 1.7 MeV was yielded. Such energies were expected to be an optimum for comparison and production of O^{3+} ions by ion-foil interaction [19].

The beam current goes through a carbon exciter foil. The foils were made from a glow discharge, had surface densities about 10-20 g/cm² and lasted for 1-2 hours under the above radiation.

VUV radiation emitted by excited oxygen ions was dispersed by a 1m Seya-Namioka grating-incidence spectrometer at about 90 degrees to the ion beam direction. A low-noise channeltron (below 1 count/m in) was served as a detector. Spectra were recorded at energies of 1.5 and 1.7 MeV with 100/100 μm slits (the line width (FWHM) was 1.1 Å) and 40/40 μm slits (the line width (FWHM) was 0.7 Å) in the wavelength range of 660-710 Å.

We also reinvestigated unpublished beam-foil spectra of $^{16}O^{3+}$, $^{19}F^{4+}$ and $^{20}Ne^{5+}$ ions recorded previously by accelerating $^{16}O^+$, $^{20}F^{H+}$ and $^{20}Ne^+$ ions to energies of 2.5 MeV, 2.5 MeV and 4.0 MeV at the University of Lyon and Argonne National Lab. The line widths (FWHM) were 0.4 Å, 0.8 Å and 0.3 Å in the wavelength range of 660-710 Å, 560-640 Å and 490-540 Å in above spectra, respectively.

III. RESULTS

Figs. 2 (a) - (c) display three typical spectra of oxygen at beam energies of 1.5, 1.7 and 2.5 MeV in the wavelength range of 660-710 Å. In the wavelength region of 665-675 Å the $1s2s2p^23p\ ^6D^o - 1s2p^33p\ ^6P$ transitions in $O\ IV$ were expected. At an O_2^+ beam energy of 1.5 MeV, O_2^+ ions are mainly excited to terms of O^{2+} and O^{3+} . There are no lines emitted from sextet states in $O\ IV$ in Fig. 2 (a). At an O^+ beam energy of 1.7 MeV, O^+ ions are mainly excited to terms of O^{3+} and O^{4+} . New and unidentified emissions appear in the spectrum in Fig. 2 (b). Fig. 2 (c) shows a spectrum with better resolution

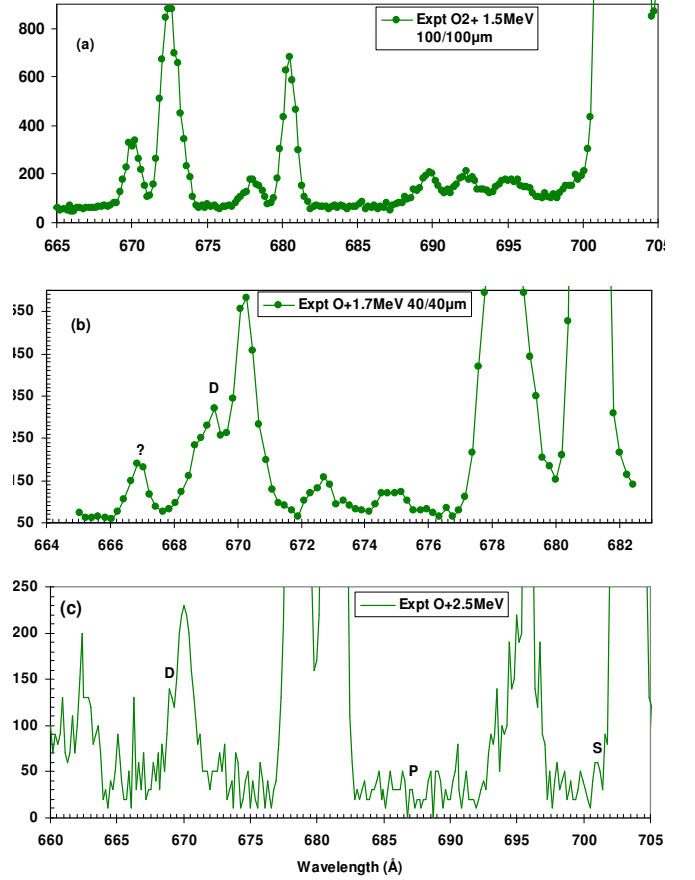


FIG. 2: Beam-foil spectra of oxygen, recorded at different energies. Units of intensities are arbitrary. Beam energies and spectrometer slit widths (in μm) are indicated. D, P and S: $1s2s2p^23p\ ^6L^o - 1s2p^33p\ ^6P_{J^o}$, $L=D, P$ and S transitions in $O\ IV$.

to see details of lines. For the $1s2s2p^23p\ ^6L^o - 1s2p^33p\ ^6P$, $L=S, P, D$ transitions we expected to partially resolve the structures of the lower states $1s2s2p^23p\ ^6L_J^o$, $L=S, P, D$ in the experiments, whereas the structures of the upper state $1s2p^33p\ ^6P_J$ are so close and less than resolution of the experimental spectra. A promising candidate for the $1s2s2p^23p\ ^6D_{9=2}^o - 1s2p^33p\ ^6P_{7=2}$ transition at 668.95 ± 0.08 Å appears in spectra recorded at 1.7 and 2.5 MeV O^+ ion beam energies (labelled as D in Figs. 2 (b) and 2 (c)), which does not appear in the spectrum recorded at 1.2 MeV O_2^+ ion beam energy. Well-known transitions of $O\ V\ 3p-4d$, $O\ IV\ 2s^23p-2s^25s$, $O\ V\ 2s3d-2s4f$ and $O\ III\ 2s^22p^2-2s2p^3$ are at 659.589 Å, 670.601 Å, 681.332 Å and 703.854 Å respectively, close to the neighborhood of the doubly excited sextet transitions. The four wavelengths have been semiempirically fitted with high accuracy of 0.004 Å by [20, 21, 22] and provided a good calibration for the measurements. Standard error for wavelength calibration is 0.01 Å in the region of 660-710 Å. Nonlinear least-squared fittings of Gaussian profiles gave values for wavelengths, intensities and

full widths at half maximum (FWHM) of lines. Uncertainties of wavelengths are related to intensities of lines. Through the use of optical refocusing we achieved spectroscopic line widths of 0.7 and 0.4 Å in Fig. 2(b) and 2(c). The precision of the plotting program was checked through several known transition wavelengths.

Multi-configuration Hartree-Fock (MCHF) method [8] with QED and higher-order relativistic corrections [1, 12, 13, 14], and Multi-configuration Dirac-Fock (MCDF) GRASP code [9, 10, 11] supported analysis of the above experimental spectra.

In MCHF approach, for a sextet state in a *ve*-electron system ($^6L, S=5/2, J_M J = (n_1 \uparrow_1^1 n_2 \uparrow_2^2 n_3 \uparrow_3^3 n_4 \uparrow_4^4 n_5 \uparrow_5^5)^6L_J, M_J$), where $w = 0, 1, \dots$, or $m = (2l+1)$, $i = 1, 2, \dots, 5$, the wavefunction is

$$(\uparrow; LS = 5/2, J) = \sum_{i=1}^N \sum_{M_J = -J}^J c_i (\uparrow_i; LS = 5/2, J_M J); \quad (1)$$

where c_i is a configuration interaction coefficient, N is total number of configurations with the same $LSJM_J$ and parity, and $(\uparrow_i; LS = 5/2, J_M J)$ is a configuration state function (CSF).

Firstly, single-configuration Hartree-Fock (SCHF) calculations where configurations are the desired levels, i.e., $1s2s2p^23p$ or $1s2p^33p$, were performed. After updating the MCHF codes, we carried out relativistic calculations with an initial expansion of up to 4000 CSFs and a full Pauli-Breit Hamiltonian matrix. For a *ve*-electron system a CI expansion generated by a active set leads to a large number of expansions. To reduce the number of configurations, we chose configurations $n_1 \uparrow_1 n_2 \uparrow_2 n_3 \uparrow_3 n_4 \uparrow_4 n_5 \uparrow_5$, where $n_i = 1, 2, 3, 4$ and 5 , $\uparrow_i = 0, \dots, m$ in $(4, n_i-1)$. We did not include *g* electrons for $n=5$ shell. For MCHF calculations of the lower states $1s2s2p^23p^6L$, $L=S, P, D$, we chose $1s, 2s, 2p, 3s, 3p, 3d, 4s, 4p, 4d$ and $5s$ electrons to compose configurations. For the $1s2p^33p^6P$ state we chose $1s$ through $4d$ electrons. Fine structure splitting is strongly involved in the experiments and identifications. After determining radial wavefunctions, we included relativistic operators of mass correction, one- and two-body Darwin terms and spin-spin contact term in both SCHF and MCHF calculations; these were not included by Miecznik et al [4].

In addition, we used the screened hydrogenic formula from [1, 12, 13, 14] to estimate quantum electrodynamic effects (QED), and higher-order relativistic contributions for sextet states in *ve*-electron oxygen, fluorine and neon.

In MCDF [9, 10, 11] approach, firstly, we used single-configuration Dirac-Fock approach (SCDF). A basis of jj-coupled states to all possible total angular momenta J from two non-relativistic configurations, $1s2s2p^23p$ and $1s2p^33p$, was considered. For convergence we included the ground state $1s^22s^22p$ of *ve*-electron systems. After calculating all possible levels for all J , eigenvectors were regrouped in a basis of LS terms. To obtain better evaluations of correlation energies of the sextet terms $1s2s2p^23p$

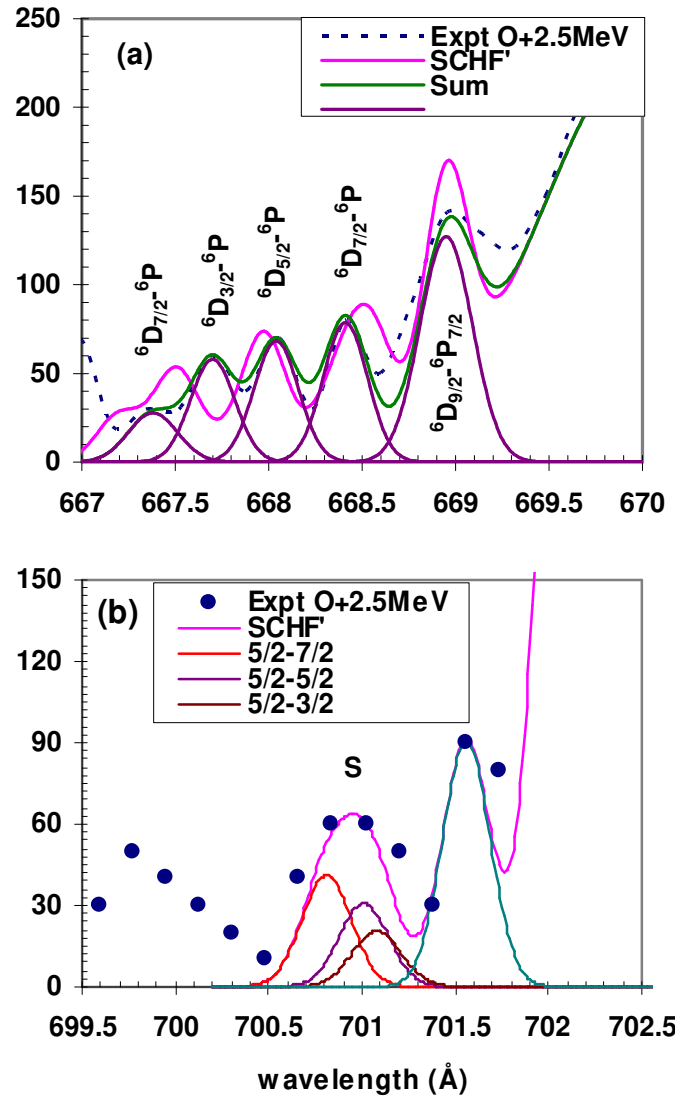


FIG. 3: Relative intensity of the $1s2s2p^23p^6D_J^o - 1s2p^33p^6P_J^o$ and $1s2s2p^23p^6S_{5=2}^o - 1s2p^33p^6P_J^o$ transitions of O IV in the experimental spectrum of oxygen at the energy of 2.5 MeV. Units of intensities are arbitrary.

6L , $L=S, P, D$ and $1s2p^33p^6P$ in O IV, F V and Ne VI, improved calculations included $1s^22s^22p, 1s^22s2p^2, 1s2s^22p^2, 1s2s2p^3, 1s2s2p^23s, 1s2s2p^23p, 1s2s2p^23d, 1s2p^33s, 1s2p^33p, 1s2p^33d, 1s2p^34s, 1s2p^34p$ and $1s2p^34d$ mixing non-relativistic configurations.

In GRASP code QED effects, self-energy and vacuum polarization correction, were taken into account by using effective nuclear charge Z_{eff} in the formulas of QED effects, which comes from an analogous hydrogenic orbital with the same expectation value of r as the MCDF-orbital in question [9, 10, 11].

Most of new identifications have been obtained by searching in the spectra for sets of unidentified lines and by comparing energies and relative intensities of the $1s2s2p^23p^6L^o - 1s2p^33p^6P$, $L=D, P$ and S transi-

tions with results of calculated by MCHF and MCDF approaches. Shown in Fig. 3(a) are details of the $1s2s2p^23p\ ^6D^{\circ}-1s2p^33p\ ^6P$ transition in O IV recorded at an O^{+} ion energy of 2.5 MeV. The curve SCHF' is convoluted theoretical profile of fine structure components with a Gaussian function. The experimental width of 0.4 Å for the oxygen spectrum was utilized. The transition rates to fine structure $j=9/3$ to $3/2$ of the lower state were results of single-configuration Hartree-Fock (SCHF) calculations by this work. The wavelengths of fine structure components were calculated SCHF results plus a fitted shift for all five components. Measured wavelength of a component is the weighted center of the fitted profile of experimental data. Experimental transition rate is proportional to area of a peak (fitted intensity FWHM of the experimental data). The curve "Sum" is summation of fitted fine structure components of experimental data. Measured ratio of $J=9/2-7/2$, $J=7/2-5/2$, $J=5/2-3/2$ and $J=3/2-1/2$ transition rates at an ion energy of 2.5 MeV in Fig. 3(a) is about 121:0.4:76:0.4:66:0.4:55:0.4:27:0.4 = 4.79:2.92:2.58:2.19:1.00. * represents all possible j s of the upper state $1s2p^33p\ ^6P_j$ allowed by electric-dipole transition rule. The ratio is slightly different from the theoretical ratio of GF values of SCHF calculations of $0.981:0.593:0.530:0.355:0.294 = 4.98:3.99:3.00:2.00:1.00$. Based on above analysis we assign the set of lines as the $1s2s2p^23p\ ^6D^{\circ}-1s2p^33p\ ^6P$ transition in O IV, and determine their wavelengths with good accuracy of 0.08 Å. The results are listed in Table I. The strongest transition related to fine structure components is the $1s2s2p^23p\ ^6D_{9=2}^{\circ}-1s2p^33p\ ^6P_{7=2}$ transition at the wavelength of 668.95 ± 0.08 Å.

Spectral details of the $1s2s2p^23p\ ^6S_{5=2}^{\circ}-1s2p^33p\ ^6P_j$ transition are shown in Fig. 3(b). The width of the line is wider than the experimental width of a resonance line of 0.4 Å, but not wide enough to resolve fine structures of the upper state $1s2p^33p\ ^6P$. In the experimental profile, experimental separation of fine structures of the upper state seems larger than results of SCHF calculations. Similar to above, after studying details of transitions theoretically and experimentally described above, and comparing with multi-configuration Hartree-Fock (MCHF) and multi-configuration Dirac-Fock (MCDF) calculations of O IV by this work, we were able to assign these unidentified observed lines as the $1s2s2p^23p\ ^6L^{\circ}-1s2p^33p\ ^6P$, $L=D, P$ and S electric-dipole transitions in O IV. Results of the identification and measurements of wavelengths of the transitions are listed in Table I. Errors of wavelengths of 0.08 Å are small mainly from calibration and curve fitting. The latter includes experimental and statistical errors. In Table I average theoretical transition energy AV is the center of gravity of the $1s2s2p^23p\ ^6L^{\circ}-1s2p^33p\ ^6P$ transition energies (computed from fine structure lines calculated by this work) with results of theoretical analysis. Experimental transition energy AV is the center of

gravity of the $1s2s2p^23p\ ^6L^{\circ}-1s2p^33p\ ^6P$ transition energies (computed from observed lines) with results of experimental transition rate analysis. AV^T is summation of above average transition energy (AV), QED effect (QED) and higher-order correction (HO). Errors for calculated transition energies in Table I are the root mean squared differences of calculated and experimental transition energies as given below in the table. We also list calculated non-relativistic transition energies ($NREL$). In Table I we present measured fine structure wavelength values and compared these with different theoretical values for O IV. The experimental results are consistent with calculations after considering experimental and theoretical errors.

Using similar experimental and theoretical analysis described above, we studied spectra recorded at a $(FH)^+$ beam energy of 2.5 MeV. Through the use of optical refocusing we achieved spectroscopic linewidth of 0.7 Å. The wavelength accuracy is 0.10 Å in the wavelength region of 570-620 Å in the spectra [23, 24]. In Table II all observed lines in the sextet system of F V are reported. Nine lines are new observations. For the $1s2s2p^23p\ ^6L-1s2p^33p\ ^6P$ transitions fine structures of the lower state $1s2s2p^23p\ ^6L$ are resolved in the experiments. The strongest fine structure component is the $1s2s2p^23p\ ^6D_{9=2}^{\circ}-1s2p^33p\ ^6P_{7=2}$ transition at the wavelength of 577.50 ± 0.10 Å.

Similarly, we studied spectra recorded at a Ne^{+} beam energy of 4.0 MeV. Through the use of optical refocusing spectroscopic linewidth of 0.3 Å was achieved in the second order spectra. Fine structures of the lower and upper state are resolved. The wavelength accuracy is 0.05 Å for the $1s2s2p^23p\ ^6L_j^{\circ}-1s2p^33p\ ^6P_{j=0}$, $L=S, P, D$ transitions in the wavelength region of 490-555 Å [25, 26]. In Table III thirteen new observed lines in the sextet system of Ne VI are reported. The strongest fine structure component is the $1s2s2p^23p\ ^6D_{9=2}^{\circ}-1s2p^33p\ ^6P_{7=2}$ transition at the wavelength of 507.13 ± 0.05 Å.

In Figs. 4, 5 and 6 are plots of differences between theoretical and experimental transition energies of the $1s2s2p^23p\ ^6L^{\circ}-1s2p^33p\ ^6P$, $L=D, P, S$ transitions along bomlike isoelectronic sequence. Here, theoretical transition energy is the center of gravity of the $1s2s2p^23p\ ^6L^{\circ}-1s2p^33p\ ^6P$ transition energies (computed from fine structure lines calculated by this work) with results of theoretical analysis, and experimental transition energy is the center of gravity of the $1s2s2p^23p\ ^6L^{\circ}-1s2p^33p\ ^6P$ transition energies (computed from observed lines) with experimental results of transition rate analysis.

In Fig. 4 calculated SCHF and SCDF transition energy differences from experiments are constant for the $1s2s2p^23p\ ^6D^{\circ}-1s2p^33p\ ^6P$ transitions for nuclear charge $Z = 8, 9$ and 10. For MCDF and non-relativistic SCHF calculations, differences are linear for nuclear charge Z

TABLE I: Energies E (in cm^{-1}) and wavelengths (in \AA) for the $1s2s2p^23p\ ^6L_J^\circ - 1s2p^33p\ ^6P_J^\circ$ transitions in O IV by this work. * represents all possible allowed J 's of the upper states by E1 transition selective rule. We list energy difference dE (in cm^{-1}) between theoretical and experimental transition energies for the $1s2s2p^23p\ ^6L_J^\circ - 1s2p^33p\ ^6P_J^\circ$ transitions.

J-J'	exp	Eexp	m chf	Em chf	dEm chf	schf	Eschf	dEschf	m cdf	Em cdf	dEm cdf	s cdf	Es cdf	dEs cdf
0.08														
1s2s2p ² 3p ⁶ D _J ^o - 1s2p ³ 3p ⁶ P _J ^o														
			32				372			710			1938	
1/2→	667.26	149867	667.36	149844	-22	668.82	149517	-350	664.15	150568	702	658.84	151782	1915
3/2→	667.70	149768	667.68	149772	4	669.12	149450	-318	664.58	150471	703	659.12	151717	1950
5/2→	668.04	149692	668.13	149671	-20	669.59	149345	-347	665.00	150376	684	659.59	151609	1918
7/2→	668.41	149609	668.54	149580	-29	670.10	149231	-377	665.64	150231	623	660.11	151490	1881
9/2-7/2	668.95	149488	669.07	149461	-27	670.57	149127	-361	666.27	150089	601	660.62	151373	1885
AV	668.34	149623	668.44	149602	-22	669.94	149267	-356	665.48	150267	644	660.66	151364	1740
QED				-23.6			-23.4							
HO				139.6			-16.7							
AV ^T			667.92	149718	95	670.12	149227	-396						
N-REL						673.61	148453	-1170						
1s2s2p ² 3p ⁶ P _J ^o - 1s2p ³ 3p ⁶ P _J ^o														
			258				555			1782			677	
3/2→	687.14	145531	685.95	145785	255	684.51	146090	559	678.94	147288	1758	675.90	147951	2420
5/2→	687.35	145486	686.23	145724	237	685.04	145977	491	679.15	147243	1757	676.18	147890	2403
7/2→	687.65	145423	686.69	145626	203	685.25	145932	509	679.91	147078	1655	676.76	147763	2340
AV	687.44	145468	686.37	145694	226	685.02	145982	514	679.44	147180	1712	676.38	147847	2379
QED				-23.5			-23.3							
HO				29.1			-39.1							
AV ^T			686.34	145700	232	685.31	145920	452						
N-REL						688.66	145209	-259						
1s2s2p ² 3p ⁶ S _J ^o - 1s2p ³ 3p ⁶ P _J ^o														
			7507				771			4252			5880	
5/2→	700.93	142668	739.86	135161	-7507	704.74	141896	-771	722.46	134216	-4252	731.06	136788	-5880
QED				-23.0			-23.1							
HO				149.3			66.7							
AV ^T			739.17	135287	-7381	704.53	141940	-728						
N-REL						708.76	141091	-1576						

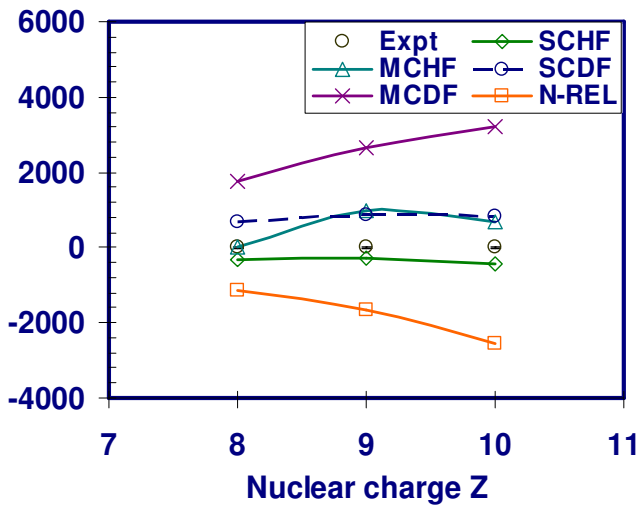


FIG .4: Difference between theoretical and experimental transition energies for the $1s2s2p^23p\ ^6D^\circ - 1s2p^33p\ ^6P$ transitions. Unit of energy difference is cm^{-1} .

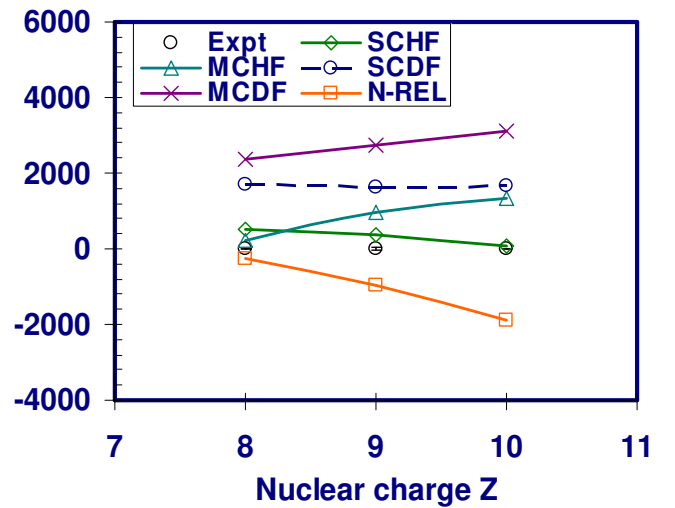


FIG .5: Difference between theoretical and experimental transition energies for the $1s2s2p^23p\ ^6P^\circ - 1s2p^33p\ ^6P$ transitions. Unit of energy difference is cm^{-1} .

TABLE II: Energies E (in cm^{-1}) and wavelengths (in \AA) for the $1s2s2p^23p\ ^6L_J^\circ - 1s2p^33p\ ^6P_J^\circ$ transitions in F V by this work. * represents all possible allowed J 's of the upper states by E1 transition selective rule. We list differences dE (in cm^{-1}) between theoretical and experimental transition energies for the $1s2s2p^23p\ ^6L_J^\circ - 1s2p^33p\ ^6P_J^\circ$ transitions.

$J-J'$	exp	Eexp	m chf	Em chf	dEm chf	schf	Eschf	dEschf	m cdf	Em cdf	dEm cdf	scdf	Escdf	dEscdf
0.10														
$1s2s2p^23p\ ^6D_J^\circ - 1s2p^33p\ ^6P_J^\circ$														
			1043				328			965			2767	
1/2-*	575.20	173853	572.17	174743	921	576.24	173539	-314	572.33	174724	872	566.42	176547	2695
3/2-*	575.85	173656	572.40	174703	1047	576.61	173427	-229	572.72	174605	949	566.77	176438	2782
5/2-*	576.43	173482	573.26	174441	959	577.23	173241	-240	573.30	174429	947	567.46	176224	2742
7/2-*	577.09	173283	573.89	174249	966	577.95	173025	-258	574.15	174171	887	568.49	175905	2621
9/2-7/2	577.50	173160	574.04	174204	1044	578.66	172813	-347	575.06	173895	735	569.01	175744	2584
AV	576.80	173369	573.50	174368	998	577.75	173085	-284	573.97	174225	855	568.09	176028	2659
QED				-41.7			-41.4							
HO				211.0			372.5							
AV ^T			572.94	174537	1168	576.65	173416	47						
N-REL						582.31	171729	-1640						
$1s2s2p^23p\ ^6P_J^\circ - 1s2p^33p\ ^6P_J^\circ$														
			1084				418			1761			2787	
3/2-*	592.45	168791	589.86	169532	741	591.01	169202	411	587.55	170198	1408	582.83	171577	2786
5/2-*	592.67	168728	589.13	169742	1014	591.26	169130	402	586.65	170459	1731	583.17	171477	2749
7/2-*	593.43	168512	589.86	169532	1020	592.16	168873	361	587.70	170155	1643	583.96	171245	2733
AV	592.96	168646	589.62	169602	956	591.60	169032	386	587.32	170266	1620	583.45	171396	2750
QED				-41.5			-41.2							
HO				216.2			343.4							
AV ^T			589.01	169777	1131	590.55	169334	688						
N-REL						596.37	167682	-964						
$1s2s2p^23p\ ^6S_J^\circ - 1s2p^33p\ ^6P_J^\circ$														
			6116				105			4418			5379	
5/2-*	615.57	162451	639.65	156335	-6116	615.97	162346	-105	632.82	158023	-4428	636.65	157072	-5379
QED				-40.7			-40.8							
HO				251.1			176.5							
AV ^T			638.79	156545	-5906	615.45	162482	31						
N-REL						620.90	161058	-1393						

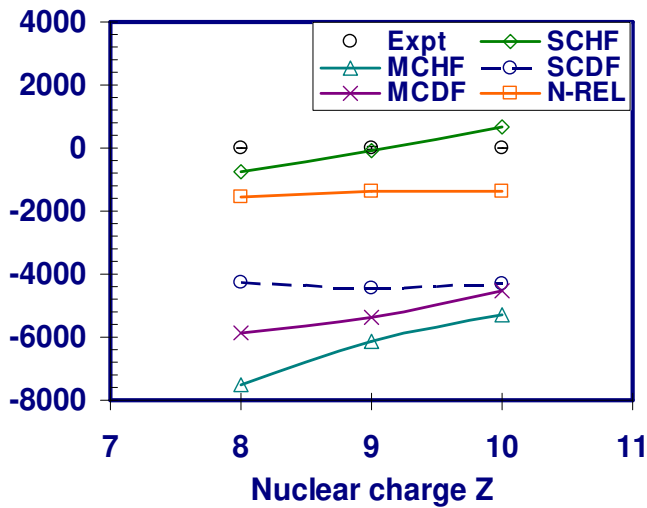


FIG. 6: Difference between theoretical and experimental transition energies for the $1s2s2p^23p\ ^6S^\circ - 1s2p^33p\ ^6P$ transitions. Unit of energy difference is cm^{-1} .

= 8, 9 and 10. For MCHF calculations for oxygen, the difference is very small, just 22 cm^{-1} .

In Fig. 5 SCDF difference is constant for the $1s2s2p^23p\ ^6P^\circ - 1s2p^33p\ ^6P$ transitions for nuclear charge $Z = 8, 9$ and 10 . MCHF, SCHF, MCDF and non-relativistic SCHF differences are linear for nuclear charge $Z = 8, 9$ and 10 . MCHF difference for oxygen is 226 cm^{-1} .

In Fig. 6 SCDF and non-relativistic SCHF differences are constant for the $1s2s2p^23p\ ^6S^\circ - 1s2p^33p\ ^6P$ transitions for nuclear charge $Z = 8, 9$ and 10 . MCHF, MCDF and SCHF differences are linear for nuclear charge $Z = 8, 9$ and 10 . SCHF difference for oxygen is 105 cm^{-1} . However, SCDF, MCHF and SCDF differences are quite large, $> 4000\text{ cm}^{-1}$ for nuclear charge $Z = 8, 9$ and 10 . In ref. [27] energy differences for transitions related to multiplet S states also show the same tendency. Above linear and constant energy differences can be used to predict easily and with high accuracy transition energies for the $1s2s2p^23p\ ^6L^\circ - 1s2p^33p\ ^6P, L = S, P, D$ transitions for boronlike ions with $5 < Z < 13$.

QED and higher-order corrections for the $1s2s2p^23p$

TABLE III: Energies E (in cm^{-1}) and wavelengths (in \AA) for the $1s2s2p^23p\ ^6L_J^\circ - 1s2p^33p\ ^6P_J^\circ$ transitions in Ne VI by this work. * represents all possible allowed J 's of the upper states by E1 transition selective rule. We list differences dE (in cm^{-1}) between theoretical and experimental transition energies for the $1s2s2p^23p\ ^6L_J^\circ - 1s2p^33p\ ^6P_J^\circ$ transitions.

J-J'	exp	Eexp	m chf	Em chf	dEm chf	schf	Eschf	dEschf	m cdf	Em cdf	dEm cdf	sodf	Esodf	dEsodf	
0.05															
1s2s2p ² 3p ⁶ D _J ^o - 1s2p ³ 3p ⁶ P _J ^o															
				917			557			1153			3497		
1/2-3/2	505.20	197941	502.64	198950		1008	505.41	197859	-82	502.07	199175	1234	496.29	201495	3554
3/2-*	505.44	197847	503.19	198732		885	505.96	197644	-203	502.50	199005	1158	496.62	201361	3514
5/2-*	505.77	197718	503.87	198464		746	506.72	197348	-371	503.40	198649	931	497.52	200997	3279
7/2-7/2	506.17	197562	504.55	198196		634	507.39	197087	-475	504.20	198334	772	498.26	200698	3136
7/2-5/2	506.50	197433	504.96	198035		602	507.78	196936	-498	504.53	198204	771	498.67	200533	3100
9/2-7/2	507.13	197188	505.78	197714		526	508.61	196614	-574	505.47	197836	648	499.53	200188	3000
AV	506.29	197517	504.56	198192		675	507.38	197089	-428	504.13	198361	844	498.23	200710	3193
QED				-68.2				-66.8							
HO				-220.0				78.9							
AV ^T			505.30	197904		387	507.35	197101	-416						
N-REL							512.88	194977	-2540						
1s2s2p ² 3p ⁶ P _J ^o - 1s2p ³ 3p ⁶ P _J ^o															
				1190			119			1832			3013		
3/2-5/2	519.53	192482	516.38	193656		1174	519.23	192593	111	514.98	194182	1701	511.58	195473	2991
3/2-3/2	519.77	192393	516.55	193592		1199	519.46	192508	115	515.21	194096	1703	511.73	195416	3023
5/2-7/2															
5/2-3/2	520.26	192212	517.20	193349		1137	520.06	192286	74	516.00	193798	1587	512.32	195191	2979
7/2-7/2	520.78	192020	517.81	193121		1101	520.74	192034	15	515.64	193934	1914	512.93	194958	2939
7/2-5/2	521.36	191806	518.24	192961		1155	521.15	191883	77	517.02	193416	1610	513.38	194787	2981
AV	520.35	192178	517.24	193333		1156	520.14	192255	77	515.72	193903	1726	512.39	195162	2984
QED				-67.8				-66.5							
HO				-50.3				-10.7							
AV ^T			517.56	193215		1037	520.35	192178	0						
N-REL							525.74	190137	-2041						
1s2s2p ² 3p ⁶ S _J ^o - 1s2p ³ 3p ⁶ P _J ^o															
				5314			735			4341			4617		
5/2-7/2	548.62	182276	564.89	177026		-5250	546.46	182996	720	561.94	177955	-4321	562.50	177778	-4498
5/2-5/2,3/2	548.94	182169	565.40	176866		-5303	546.99	182819	649	562.33	177832	-4338	563.15	177573	-4597
AV	548.80	182216	565.17	176937		-5280	546.75	182897	681	562.16	177886	-4330	562.86	177664	-4553
QED				-66.7				-66.7							
HO				-165.6				16.5							
AV ^T			565.92	176705		-5511	546.91	182847	631						
N-REL							553.04	180817	-1459						

$^6L-1s2p^33p\ ^6P^\circ$, $L=D, P$, and S transitions in O IV, F V and Ne VI are up to $-220-370\text{ cm}^{-1}$ (see Table I, II and III), and cannot be ignored in careful comparisons with experiments. We plot QED and higher-order corrections to the mean $1s2s2p^23p\ ^6L-1s2p^33p\ ^6P^\circ$, $L=D, P$, and S transition energies in Fig. 7. Here, QED and higher-order corrections are calculated from Z_{eff} values obtained from SCHF and MCHF results. For the $1s2s2p^23p\ ^6L-1s2p^33p\ ^6P^\circ$, $L=D, P$, and S transitions in O IV, F V and Ne VI, QED effects increase with Z rapidly. Results in Fig. 7 show that mean transition wavelengths are sensitive to QED effects of 0.18 \AA , 0.21 \AA and 0.22 \AA for the $1s2s2p^23p\ ^6L-1s2p^33p\ ^6P^\circ$, $L=D, P$, and S transitions in O IV, F V and Ne VI. They are at the same level or larger than the estimated experimental

precision of 0.06 \AA , 0.10 \AA and 0.05 \AA .

Some spectral lines of boronlike ions remains unidentified. In O IV notable lines at $666-668\text{ \AA}$ show stable characteristics in spectra in Fig. 2 (b) and 2 (c). Intensities measured at different ion energies indicate the figures should be classified as transitions from upper states with doubly excited cores.

IV. CONCLUSIONS

Fast beam-foil spectroscopic experiments have yielded new information on doubly excited sextet states in boronlike O IV, F V and Ne VI. We performed MCHF (with QED and higher-order corrections) and MCDFT calculations

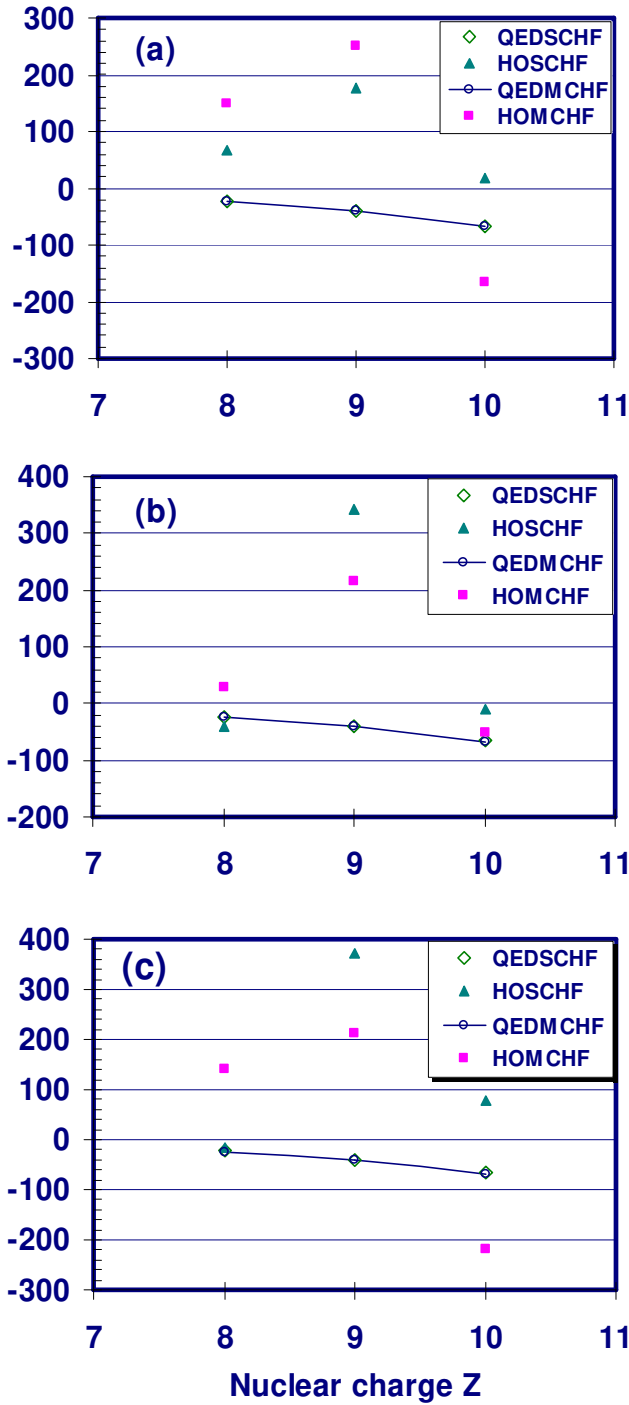


FIG. 7: Isoelectronic comparison of QED and higher-order corrections of the (a) $1s2s2p^23p\ ^6D-1s2p^33p\ ^6P^\circ$, (b) $1s2s2p^23p\ ^6P-1s2p^33p\ ^6P^\circ$ and (c) $1s2s2p^23p\ ^6S-1s2p^33p\ ^6P^\circ$ transitions for B I sequence. QED effects from SCHF and MCHF calculations are denoted by solid line. Unit of energy is cm^{-1} .

tions for 2s-2p transitions between doubly excited sextet states of ve-electron O IV, F V and Ne VI. Using calculated wavelengths and transition rates, we were able to identify observed lines in fast beam-foil spectra of oxygen, fluorine and neon corresponding to the $1s2s2p^23p\ ^6L^\circ-1s2p^33p\ ^6P$, $L=S, P, D$ electric-dipole transitions in O IV, F V and Ne VI, and to measure wavelengths with good accuracy. The measured results are compared with values of MCHD and MCDF calculations. They are in reasonable tendency. To extract QED and higher-order corrections, accurate electron correlation is required.

- [2] J.H. Blanke, B. Fricke, P.H. Heckmann and E. Trabert, Phys. Scr. 45, 430 (1992).
- [3] L. Lapierre and E. J. Knyštautas, J. Phys. B 33, 2245 (2000).
- [4] G. Miecznik, T. Brage and C.F. Fischer, Phys. Scr. 45, 436 (1992).
- [5] H.G. Berry, T. Bastin, E. Biamont, P.D. Dumont and H.P. Gamir, Rep. Prog. Phys. 5, 12 (1975).
- [6] A.E. Kramida, T. Bastin, E. Biamont, P.D. Dumont and H.P. Gamir, J. Opt. Soc. Am. B 16 (11), 1966 (1999).
- [7] K.T. Chung, Phys. Rev. A 29, 682 (1984).
- [8] C.F. Fischer, T. Brage and P. Jonsson, Computational Atomic Structure an MCHF Approach (Institute of Physics Publishing, Bristol and Philadelphia (1997)).
- [9] K.G. Dyall, and I.P. Grant, computer physics communications 55, 425 (1989).
- [10] F.A. Parpia, C.F. Fischer, and I.P. Grant, Computer Physics Communications 94 (2-3), 249 (1996).
- [11] S. Fritzsche, and I.P. Grant, Computer Physics Communications 103 (2-3), 277 (1997).
- [12] K.T. Chung, X.W. Zhu and Z.W. Wang, Phys. Rev. A 47 (3) 1740 (1992).
- [13] K.T. Chung and X.W. Zhu, Phys. Rev. A 48 (3) 1944 (1993).
- [14] G.W. F. Drake and R.A. Swainson, Phys. Rev. A 41 (3) 1243 (1990),
- [15] H.G. Berry, R.L. Brooks, K.T. Cheng, J.E. Hardis and W. Ray, Phys. Scr. 42, 391 (1982).
- [16] J.E. Hardis, H.G. Berry, L.G. Curtis and A.E. Livingston, Phys. Scr. 30, 189 (1984).
- [17] H.P. Gamir, Y. Baudinet-Robinet, and P.D. Dumont, Nuclear Instruments and Methods in Physics Research B 31, 161 (1988).
- [18] Y. Baudinet-Robinet, and P.D. Dumont, H.P. Gamir, Physica Scripta 12, 3 (1990).
- [19] R. Girardeau and E.J. Knyštautas, G. Beauchemin, Neveu R. Drouin J. Phys. B 4, 1743 (1971).
- [20] K. Bockasten and K.B. Johansson, Ark. Fys. 38, 563 (1968).
- [21] S.G. Pettersson, Phys. Scr. 26, 296 (1982).
- [22] C.E. Moore, NSRDS-NBS 3, Section 1-10 (1965-1983).
- [23] C.E. Moore, Atomic Energy Levels 1, Circ. Natl. Bur. Stand. 467 (1949).
- [24] L. Engstrom, Phys. Scr. 29, 113 (1985).
- [25] R.T. Brown, APJ 158, 829 (1969).
- [26] L.A. Vainshtein and U.I. Safronova, Phys. Scr. 31, 519 (1985).
- [27] J.H. Blanke, B. Fricke, W.-D. Sepp, P.H. Heckmann G. Moller, and C. Wagner, Phys. Scr. 42, 522 (1990).